

Photonic topological states induced by local non-Hermitian modulation

Zhihua Deng^{ID}, Dingshan Gao^{ID,*}, Jianji Dong, and Xinliang Zhang

Wuhan National Laboratory for Optoelectronics, Huazhong University of Science and Technology, Wuhan, 430074, China



(Received 17 July 2023; revised 8 October 2023; accepted 20 November 2023; published 6 December 2023)

The manipulation of topological states in topological systems can be achieved through gain-loss domain walls, offering flexibility and reconfigurability within the bulk. However, this typically necessitates a global non-Hermitian modulation, involving the modulation of all lattice points within each domain, thereby increasing the complexity of system modulation. In this study, we propose a local-non-Hermitian-modulation approach to inducing photonic topological states within topologically trivial systems. By solely modulating the lattice points along the domain boundary, we significantly reduce the complexity of modulation. We theoretically and experimentally demonstrate the generation of photonic topological states induced by local non-Hermitian modulation on a silicon chip in a one-dimensional system. This process is controlled precisely through an effective Hamiltonian. Furthermore, we extend this concept to generate higher-order topological corner states in two-dimensional systems. Our findings showcase the potential of local non-Hermitian modulation in facilitating the manipulation of photonic topological states, thereby offering new possibilities for higher-dimensional systems and other topological systems.

DOI: [10.1103/PhysRevApplied.20.064009](https://doi.org/10.1103/PhysRevApplied.20.064009)

I. INTRODUCTION

Over the past decade, the field of topological photonics has attracted considerable attention due to its potential for exploring novel physics in the context of topological phases of matter within optical systems. This research has not only revealed remarkable applications of robust and exotic topological edge states in integrated photonic devices [1–3] but has also sparked a recent surge of interest in introducing non-Hermiticity into topological systems [4–6]. The introduction of non-Hermiticity in a nonreciprocal manner leads to the intriguing phenomenon of the collapse of all eigenmodes at the domain wall, known as the non-Hermitian skin effect [7,8]. This effect has been successfully used in the development of highly efficient light funnels [9]. Conversely, when non-Hermiticity is introduced through gain and loss, it has been shown to modulate the properties of topological states, resulting in the selective enhancement of such states [10], the emergence of parity-time-symmetric topological states [11], the recovery of topological zero modes [12,13], and the realization of topological lasers [14], among other phenomena. Furthermore, gain and loss have also been used to manipulate the topological properties of Hermitian systems, leading to diverse topological phase transitions [15–25] and eliciting unique topological responses [26].

Moreover, the incorporation of gain and loss in a system presents the opportunity to create domain walls

between topologically equivalent systems, enabling flexible and reconfigurable manipulation of topological optical fields. For instance, in a one-dimensional (1D) topological waveguide array, the introduction of a suitable distribution of losses has been shown to support robust photonic zero modes at the domain wall between distinct quantum phases [27]. However, the exact topological characteristics of these zero modes remain unclear. Similarly, in a two-dimensional (2D) topological microring lattice, pump-induced gain-loss domain walls of arbitrary shapes have been discovered to harbor chiral topological edge states [28]. While this work is remarkable, the design of such topological systems can be intricate.

More recently, a simple and versatile method was proposed to construct topological states on gain-loss domain walls [29]. This method leverages an effective-Hamiltonian analysis, but it necessitates the existence of topological states within different domains. Subsequent acoustic experiments confirmed the validity of this concept [30]. In summary, the approach of introducing gain-loss domain walls offers exceptional flexibility and reconfigurability in manipulating topological states. However, it typically requires global non-Hermitian modulation, involving a large number of lattice points in 1D systems [29] or extensive arrays of lattice points in 2D systems [28–30], consequently increasing the complexity of system modulation. Therefore, it appears that this challenge could be alleviated by optimizing global non-Hermitian modulation into local non-Hermitian modulation within specific areas.

*dsgao@hust.edu.cn

In this paper, we propose an approach using local non-Hermitian modulation to generate non-Hermitian domain walls supporting photonic topological states. Specifically, we investigate the 1D Su-Schrieffer-Heeger (SSH) model and demonstrate that local non-Hermitian modulation at a single lattice point within the bulk structure greatly reduces the complexity. Through effective-Hamiltonian analysis, we observe the emergence of interface states resulting from the coupling of topological zero modes and defect zero modes at the domain wall. Non-Hermitian modulation detaches the topological zero mode and generates corresponding topological zero-energy interface states. We extend this idea to 2D systems, demonstrating the generation of higher-order topological corner states. On-chip optical simulations and experimental verification confirm the effectiveness of local non-Hermitian modulation in the 1D case. Our study presents a simple and feasible approach to realizing photonic topological states by introducing local non-Hermitian modulation in domain walls.

II. MODEL AND THEORY

We consider a 1D SSH model with intracell coupling t_1 stronger than intercell coupling t_2 [31–33]. To achieve local non-Hermitian modulation, we introduce loss γ at a single lattice point in the bulk structure, as depicted in Fig. 1(a). This lattice point, marked in red, creates a natural non-Hermitian domain wall indicated by the dashed line. The domain wall splits the SSH model into two halves, which have different structures and support different boundary states (see Sec. I in Supplemental Material [34] for details). The left part of the domain-wall structure corresponds to an open boundary of a topologically non-trivial SSH model supporting a loss-free topological zero mode ψ_T [12]. On the other hand, the right part of the domain-wall structure supports only a defect zero mode ψ_D with inherent loss. By use of the effective-Hamiltonian approach [29], the coupling between these two boundary states results in the emergence of interface states at the domain wall.

We analyze the evolution of eigenvalues as the loss coefficient γ varies, as shown in Figs. 1(b) and 1(c). As the loss increases, a pair of interface states within the band gap transform into a pair of zero-energy interface states after crossing the exceptional point [5], aligning with the concept of the effective-Hamiltonian approach. In Fig. 1(d), it is evident that the defect zero mode ψ_D becomes effectively decoupled from the topological zero mode ψ_T and becomes the primary component of the field in the defect zero-energy interface state, denoted as point *A* in the eigenspectrum. Similarly, Fig. 1(e) illustrates the effective detachment of the topological zero mode, which becomes the dominant component in the topological zero-energy interface state at point *B* in the eigenspectrum. Hence, we classify the interface state dominated by the

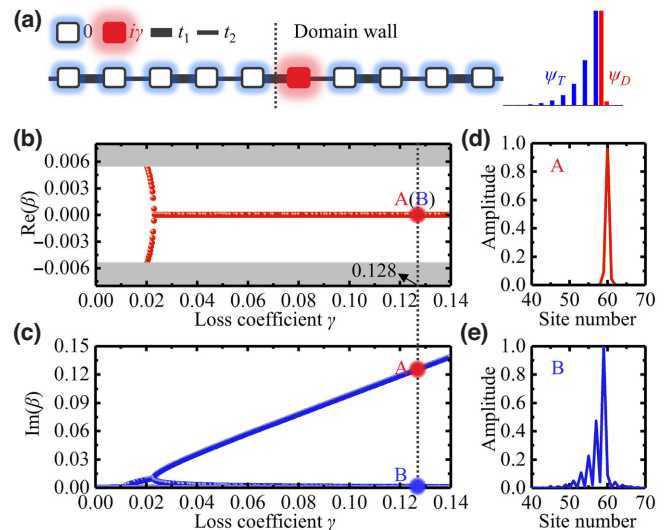


FIG. 1. (a) SSH model with the introduction of local non-Hermitian modulation. $t_1 = 0.0115$ and $t_2 = 0.0055$ are chosen. A system with 120 lattice points is considered, and the loss is placed at the 60th lattice point for illustration purposes. (b) Evolution of the real part of the eigenvalues as the loss coefficient γ varies. (c) Evolution of the imaginary part of the eigenvalues as the loss coefficient γ varies. (d) Eigenstate field distribution corresponding to point *A* at loss coefficient $\gamma = 0.128$, representing a defect zero-energy interface state. (e) Eigenstate field distribution corresponding to point *B* at loss coefficient $\gamma = 0.128$, representing a topological zero-energy interface state.

defect zero mode as the defect zero-energy interface state, while the interface state dominated by the topological zero mode is referred to as the topological zero-energy interface state.

To elucidate the mechanism of local non-Hermitian modulation, we use an effective Hamiltonian for analysis [29]. This effective Hamiltonian captures the coupling between a topological zero mode and a defect zero mode on either side of the domain wall and is mathematically defined as follows:

$$H_{\text{eff}} = \begin{bmatrix} 0 & \kappa \\ \kappa & i\chi \end{bmatrix}. \quad (1)$$

We define χ as the intrinsic loss of the defect zero mode on the right side of the domain wall, and the coupling coefficient κ represents the interaction between these two boundary states, assumed to be a real number. Solving the eigenvalue equation $H_{\text{eff}}\psi = \lambda\psi$, we obtain the eigenvalues $\lambda_{\pm} = i\chi/2 \pm \sqrt{\kappa^2 - \chi^2/4}$, and eigenstates $\psi_{\pm} = (c_{\mp}, 1)^T$, where the weight coefficient $c_{\mp} = \lambda_{\pm}/\kappa$ is involved. Thus, the interface states at the domain wall can be expressed as a combination of these eigenstates. By inverting the coupling coefficient from the eigenvalues in Figs. 1(b) and 1(c), we derive the weight coefficient based on the coupling coefficient [Fig. 2(a)]. As the loss

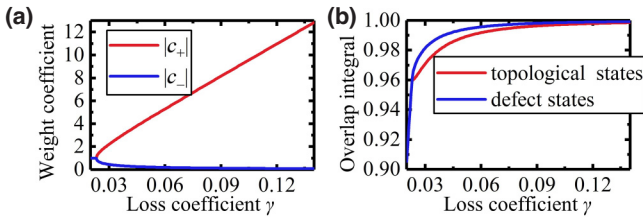


FIG. 2. (a) Spectrum of the weight coefficient as the loss coefficient γ varies. (b) Spectrum of the overlap integral as the loss coefficient γ varies. The red line represents the overlap integral between topological states, while the blue line represents the overlap integral between defect states.

increases, the weight factor c_+ rapidly increases, indicating the effective separation of the topological zero mode ψ_T from the defect zero mode ψ_D , leading to the dominance of the topological zero mode in the zero-energy interface state.

Importantly, the topological protection of the topological zero mode arises from the nontrivial Zak phase of the structure on the left side of the domain wall [12,32,33]. This protection is not affected by the structure on the right side or the presence of the defect zero mode. Consequently, the zero-energy interface state primarily composed of the topological zero mode remains topologically protected. Hence, we previously referred to it as the topological zero-energy interface state. Conversely, the corresponding interface state is the defect zero-energy interface state, primarily influenced by the defect zero mode.

To assess the validity of our method, we calculate the overlap integral between the interface states obtained with use of the effective Hamiltonian and those of the actual model in Fig. 1(a), as shown in Fig. 2(b). The overlap integral consistently exceeds 0.96 after the exceptional point, and it approaches 1 as the loss coefficient γ increases. This demonstrates strong agreement between the interface states of the actual model and those obtained by use of the effective-Hamiltonian method.

These results confirm the accuracy of the effective-Hamiltonian method in describing the physical nature of the topological zero-energy interface state generated by local non-Hermitian modulation. Notably, compared with the gain-loss-domain-wall approach [29], which requires a non-Hermitian design at multiple lattice points, our domain-wall approach necessitates only non-Hermitian control at a single lattice point. This significantly reduces the complexity of non-Hermitian modulation.

III. EXTENSION TO TWO-DIMENSIONAL SYSTEMS

Local non-Hermitian modulation can be used to generate higher-order topological corner states in 2D topological systems. We focus on the 2D SSH lattice model

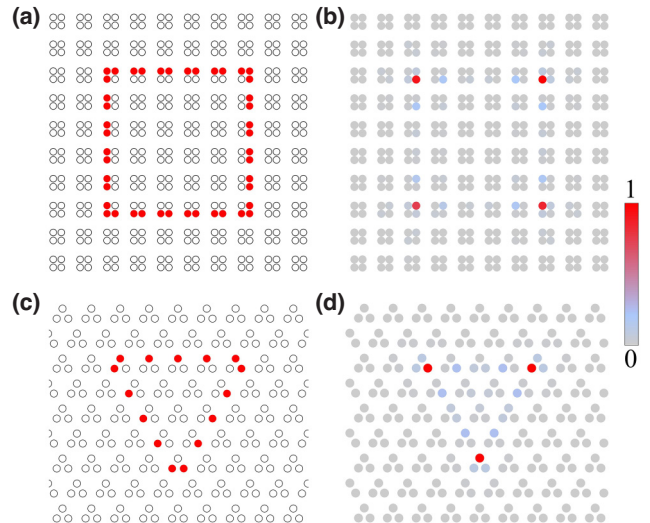


FIG. 3. (a) Trivial 2D SSH lattice model, with intracell coupling $t_1 = 4$ and intercell coupling $t_2 = 1$. (b) Calculated eigenstate of the higher-order topological corner state in the model depicted in (a) at loss coefficient $\gamma = 40$. (c) Trivial kagome-lattice model, with intracell coupling $t_1 = 4$ and intercell coupling $t_2 = 1$. (d) Calculated eigenstate of the higher-order topological corner state in the model shown in (c) at loss coefficient $\gamma = 40$.

and the kagome-lattice model [35–42], which are initially topologically trivial, as depicted in Figs. 3(a) and 3(c). In these models, corner states do not emerge unless we introduce non-Hermitian modulation. Unlike the method of constructing gain-loss domain walls, which requires explicit non-Hermitian modulation of all lattice points in different domains [29,30], our proposed approach of local non-Hermitian modulation requires modulation of only the boundaries of the domains.

As illustrated in Figs. 3(a) and 3(c), we introduce loss modulation at the red lattice points. The modulation introduces non-Hermitian domain walls, which have different internal and external structures (see Sec. I in Supplemental Material [34] for details). It is evident that the enclosed boundaries formed by the modulation preserve the structure of the topologically nontrivial 2D SSH lattice model [Fig. 3(a)] and the topologically nontrivial kagome-lattice model [Fig. 3(c)] [35,36,41]. The introduction of loss modulation effectively separates the corner states supported by the internal structures, as demonstrated in Figs. 3(b) and 3(d).

Compared with the gain-loss-domain-wall approach, which requires modulation of a number of lattice points proportional to N^2 , our local non-Hermitian modulation requires modulation of only a number of lattice points proportional to N . This transition from a quadratic to a linear relationship significantly reduces the complexity of the modulation process.

IV. OPTICAL SIMULATIONS AND EXPERIMENTAL VERIFICATION

We conducted simulations and experiments using 1D subwavelength-grating- (SWG) waveguide arrays to verify the photonic topological states generated by local non-Hermitian modulation in a 1D system [25,43,44]. As depicted in Fig. 4(a), we experimentally fabricated SWG-waveguide arrays on a commercial silicon-on-insulator wafer with a 220-nm-thick top layer of silicon using electron-beam lithography and inductively-coupled plasma etching. This fabrication allowed us to realize the model shown in Fig. 1(a).

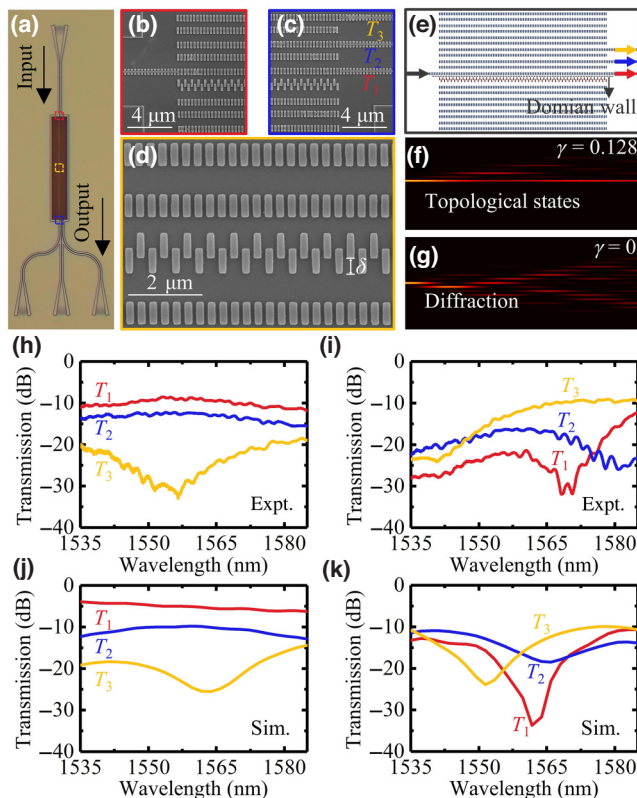


FIG. 4. (a) Microscope image showcasing the fabricated SWG-waveguide array. (b) SEM image of the input port. (c) SEM image of the output port. (d) SEM image highlighting the domain wall in the waveguide array. (e) Simulated waveguide array. (f) FDTD simulation illustrating the optical field evolution with local non-Hermitian modulation and loss coefficient $\gamma = 0.128$. (g) FDTD simulation depicting the optical field evolution without local non-Hermitian modulation. (h) Experimental optical field transmission spectrum with local non-Hermitian modulation and loss coefficient $\gamma = 0.128$. (i) Experimental optical field transmission spectrum without local non-Hermitian modulation. (j) Optical field transmission spectrum obtained from FDTD simulation (sim.) with local non-Hermitian modulation and loss coefficient $\gamma = 0.128$. (k) Optical field transmission spectrum obtained from FDTD simulation without local non-Hermitian modulation.

To detect the output optical field transmittance and determine the presence of the local non-Hermitian modulation-induced photonic topological state, we used a single-waveguide-input-excitation method [32,33]. Three output waveguides were used to measure the transmittance (T_1 , T_2 , T_3) of the output optical field. The top-view scanning-electron-microscopy (SEM) images of the input port and the output port are shown in Figs. 4(b) and 4(c), respectively. The coupling coefficients of the model in Fig. 1(a) were obtained by our modulating the waveguide spacings, while the loss coefficient was obtained by our adjusting the corrugation amplitude (δ) of the lossy SWG waveguide, as illustrated in Fig. 4(d) [25,43,44]. The design wavelength was set at 1550 nm, and specific structural parameters can be found in Supplemental Material [34].

We developed a finite-difference time-domain (FDTD) simulation model to further investigate the system. As illustrated in Fig. 4(e), the lossy SWG waveguide is highlighted in red. In the simulation, we used a single-waveguide input located on the nonlossy side of the domain wall to excite the photonic topological state. Figure 4(f) demonstrates the simulated optical field evolution at 1550 nm when non-Hermitian modulation is introduced with loss coefficient $\gamma = 0.128$. The results show a clear localization of the optical field, indicating the excitation of a topological zero-energy interface state depicted in Fig. 1(e). In contrast, when there is no local non-Hermitian modulation, the system corresponds to the Hermitian trivial SSH model, and it does not support topological states. As depicted in Fig. 4(g), the incident light excites the bulk state and is diffracted.

To validate the reliability of our FDTD optical simulation, we also conducted simulations of the optical field evolution based on coupled-mode theory using the same parameters (see Sec. III in Supplemental Material [34] for details). The results are consistent with the FDTD simulation, confirming the feasibility of our optical design.

To validate our findings, we conducted experimental tests on the fabricated chips to measure the optical field transmission. When applying localized non-Hermitian modulation with loss coefficient $\gamma = 0.128$, as shown in Fig. 4(h), we observed that $T_1 > T_2 > T_3$ between 1535 and 1585 nm, indicating a significant localization of the optical field. This experimental result aligns with the corresponding simulation results depicted in Fig. 4(j), confirming the generation of the photonic topological state.

In contrast, when no non-Hermitian modulation was present, as shown in Fig. 4(i), we observed that ports 2 and 3 dominated the output optical field, indicating scattering into the bulk structure. This observation is consistent with the corresponding simulation result displayed in Fig. 4(k).

In conclusion, we have successfully demonstrated the feasibility of generating photonic topological states through local non-Hermitian modulation using 1D

non-Hermitian SWG-waveguide arrays. It is important to note that our experimental verification has been limited to the 1D case due to platform and technological constraints. However, we anticipate that the 2D case can be experimentally validated by designing 2D waveguide arrays using the direct laser-writing technique [45], where loss can be introduced through optical field radiation leakage generated by the wiggling waveguide.

V. CONCLUSION

We have demonstrated, both theoretically and experimentally in a 1D system, that the photonic topological state can be induced by local non-Hermitian modulation, accurately described by an effective Hamiltonian. This approach simplifies the modulation process by requiring modulation at only one lattice point, making it easier to implement compared with the gain-loss-domain-wall scheme. Furthermore, we have extended this concept to generate higher-order topological corner states in 2D systems, significantly reducing the number of modulated lattice points compared with the gain-loss-domain-wall scheme. Our local non-Hermitian modulation provides a simpler method for manipulating topological states within the bulk structure of a system.

We believe that the concept of local non-Hermitian modulation has the potential to be extended to three-dimensional or higher-dimensional systems, leading to the generation of even more intriguing topological states. Additionally, we anticipate that this idea is not limited to optical systems alone, but may also provide insights and inspiration for other physical systems.

ACKNOWLEDGMENTS

This work was supported by the National Natural Science Foundation of China (Grants No. 61975062 and No. U21A20511) and the Innovation Fund of Wuhan National Laboratory for Optoelectronics, China.

- [1] T. Ozawa, H. M. Price, A. Amo, N. Goldman, M. Hafezi, L. Lu, M. C. Rechtsman, D. Schuster, J. Simon, O. Zilberberg, and Iacopo Carusotto, Topological photonics, *Rev. Mod. Phys.* **91**, 015006 (2019).
- [2] H. Price *et al.*, Roadmap on topological photonics, *J. Phys.: Photonics* **4**, 032501 (2022).
- [3] Y. Wu, C. Li, X. Hu, Y. Ao, Y. Zhao, and Q. Gong, Applications of topological photonics in integrated photonic devices, *Adv. Opt. Mater.* **5**, 1700357 (2017).
- [4] K. Kawabata, K. Shiozaki, M. Ueda, and M. Sato, Symmetry and topology in non-Hermitian physics, *Phys. Rev. X* **9**, 041015 (2019).
- [5] E. J. Bergholtz, J. C. Budich, and F. K. Kunst, Exceptional topology of non-Hermitian systems, *Rev. Mod. Phys.* **93**, 015005 (2021).
- [6] Q. Wang and Y. Chong, Non-Hermitian photonic lattices: Tutorial, *JOSA B* **40**, 1443 (2023).
- [7] S. Yao and Z. Wang, Edge states and topological invariants of non-Hermitian systems, *Phys. Rev. Lett.* **121**, 086803 (2018).
- [8] C. Scheibner, W. T. Irvine, and V. Vitelli, Non-Hermitian band topology and skin modes in active elastic media, *Phys. Rev. Lett.* **125**, 118001 (2020).
- [9] S. Weidemann, M. Kremer, T. Helbig, T. Hofmann, A. Stegmaier, M. Greiter, R. Thomale, and A. Szameit, Topological funneling of light, *Science* **368**, 311 (2020).
- [10] C. Poli, M. Bellec, U. Kuhl, F. Mortessagne, and H. Schomerus, Selective enhancement of topologically induced interface states in a dielectric resonator chain, *Nat. Commun.* **6**, 6710 (2015).
- [11] S. Weimann, M. Kremer, Y. Plotnik, Y. Lumer, S. Nolte, K. G. Makris, M. Segev, M. C. Rechtsman, and A. Szameit, Topologically protected bound states in photonic parity-time-symmetric crystals, *Nat. Mater.* **16**, 433 (2017).
- [12] W. Song, W. Sun, C. Chen, Q. Song, S. Xiao, S. Zhu, and T. Li, Breakup and recovery of topological zero modes in finite non-Hermitian optical lattices, *Phys. Rev. Lett.* **123**, 165701 (2019).
- [13] Z. Gu, H. Gao, T. Liu, S. Liang, S. An, Y. Li, and J. Zhu, Topologically protected exceptional point with local non-Hermitian modulation in an acoustic crystal, *Phys. Rev. Appl.* **15**, 014025 (2021).
- [14] Y. Ota, K. Takata, T. Ozawa, A. Amo, Z. Jia, B. Kante, M. Notomi, Y. Arakawa, and S. Iwamoto, Active topological photonics, *Nanophotonics* **9**, 547 (2020).
- [15] K. Takata and M. Notomi, Photonic topological insulating phase induced solely by gain and loss, *Phys. Rev. Lett.* **121**, 213902 (2018).
- [16] X.-W. Luo and C. Zhang, Higher-order topological corner states induced by gain and loss, *Phys. Rev. Lett.* **123**, 073601 (2019).
- [17] H. Gao, H. Xue, Q. Wang, Z. Gu, T. Liu, J. Zhu, and B. Zhang, Observation of topological edge states induced solely by non-Hermiticity in an acoustic crystal, *Phys. Rev. B* **101**, 180303 (2020).
- [18] S. Liu, S. Ma, C. Yang, L. Zhang, W. Gao, Y. J. Xiang, T. J. Cui, and S. Zhang, Gain-and loss-induced topological insulating phase in a non-Hermitian electrical circuit, *Phys. Rev. Appl.* **13**, 014047 (2020).
- [19] H. Gao, H. Xue, Z. Gu, T. Liu, J. Zhu, and B. Zhang, Non-Hermitian route to higher-order topology in an acoustic crystal, *Nat. Commun.* **12**, 1888 (2021).
- [20] H. Wu, L. Jin, and Z. Song, Topology of an anti-parity-time symmetric non-Hermitian Su-Schrieffer-Heeger model, *Phys. Rev. B* **103**, 235110 (2021).
- [21] J.-R. Li, L.-L. Zhang, W.-B. Cui, and W.-J. Gong, Topological properties in non-Hermitian tetratomic Su-Schrieffer-Heeger lattices, *Phys. Rev. Res.* **4**, 023009 (2022).
- [22] Q. Mo, Y. Sun, J. Li, Z. Ruan, and Z. Yang, Imaginary-disorder-induced topological phase transitions, *Phys. Rev. Appl.* **18**, 064079 (2022).
- [23] G. Xu, Y. Yang, X. Zhou, H. Chen, A. Alù, and C.-W. Qiu, Diffusive topological transport in spatiotemporal thermal lattices, *Nat. Phys.* **18**, 450 (2022).

- [24] B. Zhu, L.-J. Lang, Q. Wang, Q. J. Wang, and Y. Chong, Topological transitions with an imaginary Aubry-Andre-Harper potential, *Phys. Rev. Res.* **5**, 023044 (2023).
- [25] Z. Deng, D. Gao, J. Dong, and X. Zhang, On-chip loss-modulated photonic topological edge states in anti- \mathcal{PT} -symmetric waveguide arrays, *Phys. Rev. Appl.* **20**, 044019 (2023).
- [26] Y. G. Liu, P. S. Jung, M. Parto, D. N. Christodoulides, and M. Khajavikhan, Gain-induced topological response via tailored long-range interactions, *Nat. Phys.* **17**, 704 (2021).
- [27] M. Pan, H. Zhao, P. Miao, S. Longhi, and L. Feng, Photonic zero mode in a non-Hermitian photonic lattice, *Nat. Commun.* **9**, 1308 (2018).
- [28] H. Zhao, X. Qiao, T. Wu, B. Midya, S. Longhi, and L. Feng, Non-Hermitian topological light steering, *Science* **365**, 1163 (2019).
- [29] Y. Li, C. Fan, X. Hu, Y. Ao, C. Lu, C. Chan, D. M. Kennes, and Q. Gong, Effective Hamiltonian for photonic topological insulator with non-Hermitian domain walls, *Phys. Rev. Lett.* **129**, 053903 (2022).
- [30] H. Fan, H. Gao, T. Liu, S. An, X. Kong, G. Xu, J. Zhu, C.-W. Qiu, and Z. Su, Reconfigurable topological modes in acoustic non-Hermitian crystals, *Phys. Rev. B* **107**, L201108 (2023).
- [31] W. Su, J. Schrieffer, and A. J. Heeger, Solitons in polyacetylene, *Phys. Rev. Lett.* **42**, 1698 (1979).
- [32] Q. Cheng, Y. Pan, Q. Wang, T. Li, and S. Zhu, Topologically protected interface mode in plasmonic waveguide arrays, *Laser Photon. Rev.* **9**, 392 (2015).
- [33] A. Blanco-Redondo, I. Andonegui, M. J. Collins, G. Harari, Y. Lumer, M. C. Rechtsman, B. J. Eggleton, and M. Segev, Topological optical waveguiding in silicon and the transition between topological and trivial defect states, *Phys. Rev. Lett.* **116**, 163901 (2016).
- [34] See Supplemental Material at <http://link.aps.org/supplemental/10.1103/PhysRevApplied.20.064009> for different structures on both sides of the domain wall, simulation parameters, and transmission properties based on coupled-mode theory.
- [35] B. Xie, H.-X. Wang, X. Zhang, P. Zhan, J.-H. Jiang, M. Lu, and Y. Chen, Higher-order band topology, *Nat. Rev. Phys.* **3**, 520 (2021).
- [36] M. Ezawa, Higher-order topological insulators and semimetals on the breathing kagome and pyrochlore lattices, *Phys. Rev. Lett.* **120**, 026801 (2018).
- [37] X.-D. Chen, W.-M. Deng, F.-L. Shi, F.-L. Zhao, M. Chen, and J.-W. Dong, Direct observation of corner states in second-order topological photonic crystal slabs, *Phys. Rev. Lett.* **122**, 233902 (2019).
- [38] A. El Hassan, F. K. Kunst, A. Moritz, G. Andler, E. J. Bergholtz, and M. Bourennane, Corner states of light in photonic waveguides, *Nat. Photonics* **13**, 697 (2019).
- [39] M. Li, D. Zhirihi, M. Gorlach, X. Ni, D. Filonov, A. Slobozhanyuk, A. Alù, and A. B. Khanikaev, Higher-order topological states in photonic kagome crystals with long-range interactions, *Nat. Photonics* **14**, 89 (2020).
- [40] X. Ni, M. Weiner, A. Alù, and A. B. Khanikaev, Observation of higher-order topological acoustic states protected by generalized chiral symmetry, *Nat. Mater.* **18**, 113 (2019).
- [41] B.-Y. Xie, G.-X. Su, H.-F. Wang, H. Su, X.-P. Shen, P. Zhan, M.-H. Lu, Z.-L. Wang, and Y.-F. Chen, Visualization of higher-order topological insulating phases in two-dimensional dielectric photonic crystals, *Phys. Rev. Lett.* **122**, 233903 (2019).
- [42] H. Xue, Y. Yang, F. Gao, Y. Chong, and B. Zhang, Acoustic higher-order topological insulator on a kagome lattice, *Nat. Mater.* **18**, 108 (2019).
- [43] Q. Liu, S. Li, B. Wang, S. Ke, C. Qin, K. Wang, W. Liu, D. Gao, P. Berini, and P. Lu, Efficient mode transfer on a compact silicon chip by encircling moving exceptional points, *Phys. Rev. Lett.* **124**, 153903 (2020).
- [44] W. Liu, Y. Zhang, Z. Deng, J. Ye, K. Wang, B. Wang, D. Gao, and P. Lu, On-chip chiral mode switching by encircling an exceptional point in an anti-parity-time symmetric system, *Laser Photon. Rev.* **16**, 2100675 (2022).
- [45] O. Zilberberg, S. Huang, J. Guglielmon, M. Wang, K. P. Chen, Y. E. Kraus, and M. C. Rechtsman, Photonic topological boundary pumping as a probe of 4D quantum hall physics, *Nature* **553**, 59 (2018).